On the Unimportance of Phase-Coherent Measurements for Beampattern-Assisted Positioning

Josef Kulmer*, Stefan Grebien*, Michael Rath, Klaus Witrisal

Graz University of Technology, Austria

email: kulmer@tugraz.at

Abstract—**Accurate indoor radio positioning requires high-resolution measurements to either utilize or mitigate the impact of multipath propagation. This high resolution can be achieved using large signal-bandwidth, leading to superior time resolution and / or multiple antennas, leading to additional angle resolution. To facilitate multiple antennas, phase-coherent measurements are typically necessary. In this work we propose to employ non-phase-coherent measurements obtained from directional antennas for accurate single-anchor indoor positioning. The derived algorithm exploits beampatterns to jointly estimate multipath amplitudes to be used in maximum likelihood position estimation. Our evaluations based on measured and computer generated data demonstrate only a minor degradation in comparison to a phase-coherent processing scheme.**

I. INTRODUCTION

Robust and accurate indoor radio positioning can be provided by (ultra-) wideband (UWB) measurements, making use of the time-of-arrival of the line-of-sight (LOS) component [1], [2]. Depending on the bandwidth of the employed signal, multipath propagation distorts the received signal, leading to wrong time-of-arrival and subsequently position estimates [2]. By increasing the bandwidth, it is not only possible to increase the time-resolution, leading to a more separated LOS component, but also to estimate the time-of-arrival of specular multipath components (MPC), resulting from reflections at objects in the room, e.g. walls and windows [3]. These specular MPCs can be used for positioning if a geometric model of the environment is used as prior information. However, these specular components are influenced by path-overlap, i.e. different MPCs arriving at the same time, making the estimation process troublesome.

To overcome effects from path-overlap, antenna arrays [4] are beneficial due to their additional spatial information. Alternatively, the employment of directional antennas has shown increased positioning accuracy, using received signal strength [5] or UWB ranging [6]. Recently, it has been shown that utilizing an array of directional antennas at the base station can enhance multipath-resolved positioning as well [7]. The directionality of the antennas can be used to jointly estimate the amplitudes of the LOS and the specular MPCs. To employ the method derived in [7], phase-coherent measurements are necessary for the different antennas.
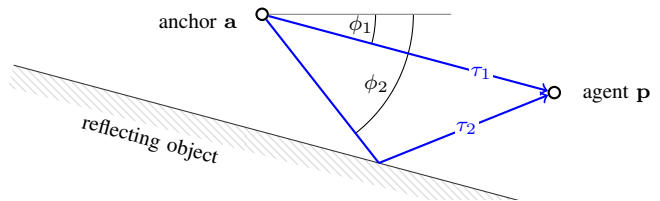
Fig. 1. Illustration of geometry model for specular reflections between anchor position **a** and agent position **p**. The multipath components $k = 1, 2$ are characterized by delays τ_1, τ_2 and angles ϕ_1, ϕ_2.

Low cost UWB tranceivers like the BeSpoon UM100 [8] or the DecaWave DW1000 [9] enable the usage of high bandwidths for battery powered sensors enabling applications like ambient assisted living, autonomous navigation or asset tracking [10]. While laboratory-grade measurement equipment, e.g., vector network analyzers, provide phase-coherent processing, these low-cost UWB chipsets are not able to maintain a stable phase-lock for more than a single measurement. Thus, the previously developed methods which require phase-coherency cannot be employed directly.

The main contributions of this paper are:
- We formulate algorithms for directional antennas based on phase-coherent / non-phase-coherent processing.
- We derive a single-anchor positioning algorithm utilizing non-phase-coherent amplitude estimates.
- We evaluate the proposed, the phase-coherent, and the non-phase-coherent position estimator and compare the results to the Cramér Rao lower bound.
- We show the applicability to real measured data.

An implementation of the proposed positioning algorithm and the used data set are available to the research community at *http://www2.spsc.tugraz.at/people/s0773094/WCNC2017/*

II. SIGNAL MODEL AND POSITION ESTIMATE

We consider the propagation channel between an anchor at position **a** and an agent at position **p**. The anchor is equipped with M antennas where $b_m(\phi)$ is the complex-valued beampattern of the mth antenna for direction ϕ. The agent employs a single-antenna with a uniform radiation pattern. We model the baseband equivalent propagation channel for the mth antenna as tapped delay line

$$h_m(t) = \sum_{k=1}^{K} b_m(\phi_k)\alpha_k\delta(t - \tau_k) \tag{1}$$

where K is the number of multipath components, α_k, τ_k and ϕ_k are the complex-valued amplitude, propagation delay and direction of the kth MPC, and $\delta(t)$ is the Dirac delta function with time t. Note, the MPC parameters are independent of the used antenna. The impact of the antenna is described by the beampattern $b_m(\phi_k)$ only.

Our objective is the estimation of the agent position $\mathbf{p}$ using measured channel impulse responses. To ensure robust positioning we require an immediate connection between $\mathbf{p}$ and channel measurements. We do not estimate the MPC parameters angle and delay from the channel measurements. In this paper we derive likelihood functions which compare channel measurements with parameters of channel models. The likelihoods are solely parameterized by hypothesized agent positions. Still, linking the channel model to hypothesized agent positions requires appropriate descriptions of the MPC parameters τ_k, ϕ_k and α_k.

Starting with delays τ_k and angles ϕ_k, we employ a geometry model as introduced in [11], [12] and [13]. The geometry model describes the wave propagation as rays, traveling from $\mathbf{a}$ to $\mathbf{p}$ as illustrated in Figure 1. Hereby, we consider specular reflections at objects and neglect propagation effects like diffraction or penetration. Each specular reflection conveys position-related information which can be recursively used to estimate the agent position [13, Appendix A]. The example in Figure 1 provides two MPCs, a line-of-sight ($k = 1$) and one specular reflection ($k = 2$) originating at the reflective surface. Knowledge of the location of the reflective surface enables to estimate the agent position $\mathbf{p}$ using the MPC parameters of the line-of-sight τ_1, ϕ_1 and of the reflection τ_2, ϕ_2.

Relating the remaining MPC parameter α_k to agent and anchor positions is not straightforward. Similar to [13] we refrain from modeling the MPC amplitudes (e.g. using path loss models). In contrast to τ_k and ϕ_k, the amplitudes are the only MPC parameters which are estimated from channel measurements.

A. Signal model

Absence of a proper model for MPC amplitudes requires their accurate estimation. In [7] the authors have estimated the MPC amplitudes jointly, incorporating information from all M channels. The joint estimation requires phase-coherent processing, i.e. adjacent measurements are phase-coherent which requires the synchronization of the transmitting and receiving clocks. Although phase-coherent processing is nowadays provided by state-of-the-art measurement equipment, low-cost transceivers are not able to maintain a stable phase-lock for more than a single measurement. Adjacent measurements are characterized by a phase offset which affects the estimation of α_k. We emphasize explicitly the phase offset of the mth antenna as a constant $e^{j\varphi_m}$. Then, the received signal can be denoted as

$$r_m(t) = e^{j\varphi_m} \sum_{k=1}^{K} b_m(\phi_k)\alpha_k s(t - \tau_k) + w_m(t), \quad (2)$$

where $s(t)$ denotes the band-limited transmitted signal and $w_m(t)$ is additive, white Gaussian noise with a double-sided

power spectral density of $N_0/2$. Sampling of (2) with sampling period T_s yields

$$r_m[n] = e^{j\varphi_m} \sum_{k=1}^{K} b_m(\phi_k)\alpha_k s_{\tau_k}[n] + w_m[n] \quad (3)$$

with sampled measurement $r_m[n] = r_m(nT_s)$, delayed transmitted signal $s_\tau[n] = s(nT_s - \tau)$ and measurement noise $w_m[n] = w_m(nT_s)$ with variance $\sigma^2 = N_0/T_s$.

In the following we formulate a position estimator based on the maximum likelihood (ML) criterion, using (3). We start by formulating a non-phase-coherent likelihood function for a single-antenna measurement (Section II-B) and proceed with a phase-coherent likelihood function for multiple antennas (Sec. II-C1).

B. Non-phase-coherent ML estimate

1) Likelihood function for single-antenna: Having a single-antenna measurement available, we can rewrite (3) in matrix-vector notation as

$$\mathbf{r}_m = e^{j\varphi_m}\mathbf{X}_m\boldsymbol{\alpha} + \mathbf{w}_m \quad (4)$$

where

$$\mathbf{r}_m = [r_m[0], r_m[1], \ldots, r_m[N-1]]^T \in \mathbb{C}^{N \times 1}$$
$$\mathbf{s}_{\tau_k} = [s_{\tau_k}[0], s_{\tau_k}[1], \ldots, s_{\tau_k}[N-1]]^T \in \mathbb{C}^{N \times 1}$$
$$\mathbf{X}_m = [b_m(\phi_1)\mathbf{s}_{\tau_1}, \ldots, b_m(\phi_K)\mathbf{s}_{\tau_K}] \in \mathbb{C}^{N \times K}$$
$$\boldsymbol{\alpha} = [\alpha_1, \ldots, \alpha_K]^T \in \mathbb{C}^{K \times 1}$$
$$\mathbf{w}_m = [w_m[0], w_m[1], \ldots, w_m[N-1]]^T \in \mathbb{C}^{N \times 1}$$

and

$$\boldsymbol{\tau} = [\tau_1, \ldots, \tau_K]^T \in \mathbb{R}^{K \times 1}, \boldsymbol{\phi} = [\phi_1, \ldots, \phi_K]^T \in \mathbb{R}^{K \times 1}$$

with measurement length N. Throughout this section we aim at estimating the MPC amplitudes from channel measurements. We admit that having only a single-antenna measurement at hand there are ambiguous solutions for phase-offset and MPC amplitudes. The phase-offset appears as constant phase error in the amplitude estimates and thus, only their product $e^{j\varphi_m}\boldsymbol{\alpha}$ can be estimated explicitly. Let

$$\boldsymbol{\alpha}_m = e^{j\varphi_m}\boldsymbol{\alpha} \quad (5)$$

with entries $\boldsymbol{\alpha}_m = [\alpha_{1,m}, \ldots, \alpha_{K,m}]^T$ be the amplitudes $\alpha_{k,m} = e^{j\varphi_m}\alpha_k$ containing the phase-offset. Then the values in $\mathbf{r}_m$ are distributed as complex Normal $\mathcal{N}(\mathbf{X}_m\boldsymbol{\alpha}_m, \sigma^2\mathbf{I}_{N \times N})$ with $\mathbf{I}_{N \times N}$ denoting the N-dimensional identity matrix. The probability density function in log domain follows as

$$\log p(\mathbf{r}_m) = -N \log(\pi\sigma^2)$$
$$-\frac{1}{\sigma^2}(\mathbf{r}_m - \mathbf{X}_m\boldsymbol{\alpha}_m)^H(\mathbf{r}_m - \mathbf{X}_m\boldsymbol{\alpha}_m). \quad (6)$$

Neglecting the constants, a log likelihood function L^{sa} for single-antenna measurements would be

$$L^{\text{sa}}(\mathbf{r}_m; \boldsymbol{\alpha}_m, \boldsymbol{\tau}, \boldsymbol{\phi}) = -\frac{1}{\sigma^2}(\mathbf{r}_m - \mathbf{X}_m\boldsymbol{\alpha}_m)^H(\mathbf{r}_m - \mathbf{X}_m\boldsymbol{\alpha}_m)$$
$$(7)$$

where we identify the phase-offset and MPC parameters as the unknowns in the log likelihood function.

We propose to estimate $\hat{\boldsymbol{\alpha}}_m$ conditioned on $\boldsymbol{\tau}$ and $\boldsymbol{\phi}$ by maximization of the log likelihood function according to

$$\frac{\partial L^{\mathrm{sa}}(\mathbf{r}_m; \boldsymbol{\alpha}_m, \boldsymbol{\tau}, \boldsymbol{\phi})}{\partial \boldsymbol{\alpha}_m} = \frac{-2}{\sigma^2}(\mathbf{X}_m^H \mathbf{r}_m - \mathbf{X}_m^H \mathbf{X}_m \boldsymbol{\alpha}_m). \quad (8)$$

Setting the derivative to zero, the ML solution $\hat{\boldsymbol{\alpha}}_m^{\mathrm{sa}}$ results in

$$\hat{\boldsymbol{\alpha}}_m^{\mathrm{sa}} = (\mathbf{X}_m^H \mathbf{X}_m)^{-1} \mathbf{X}_m^H \mathbf{r}_m. \quad (9)$$

In the special case of non-overlapping MPCs, i.e. $\mathbf{s}_{\tau_1}^H \mathbf{s}_{\tau_2} = 0$ for any $\tau_1 \neq \tau_2$, the amplitudes $\hat{\boldsymbol{\alpha}}_m^{\mathrm{sa}} = [\hat{\alpha}_{1,m}^{\mathrm{sa}}, \ldots, \hat{\alpha}_{K,m}^{\mathrm{sa}}]$ in (9) can be calculated independently according to

$$\hat{\alpha}_{k,m}^{\mathrm{sa}} = \frac{b_m^*(\phi_k)}{|b_m(\phi_k)|^2} \frac{\mathbf{s}_{\tau_k}^H \mathbf{r}_m}{\|\mathbf{s}_{\tau_k}\|^2} \quad (10)$$

demonstrating the impact of the beampattern on the estimation of $\hat{\alpha}_{k,m}^{\mathrm{sa}}$. Plugging (4) in (10) demonstrates that the amplitude estimate attains the true one according to

$$\hat{\alpha}_{k,m}^{\mathrm{sa}} = \alpha_{k,m} + \frac{1}{b_m(\phi_k)} \frac{\mathbf{s}_{\tau_k}^H \mathbf{w}_m}{\|\mathbf{s}_{\tau_k}\|^2}. \quad (11)$$

Note, we can identify the second term on the right-hand-side of (11) as error term calculated as projection of the additive noise $\mathbf{w}_m$ on the normalized transmitted signal $\mathbf{s}_{\tau_k}/\|\mathbf{s}_{\tau_k}\|^2$. Its scaling by the inverse of the beampattern can be interpreted as an undesired noise gain. We can conclude that MPCs with arriving angles ϕ within the antenna's mainlobe ($|b(\phi)|$ is large) are subject to less interference by additive noise, as illustrated in Figure 2.

Using an appropriate geometry model, the MPC parameters τ_k and ϕ_k in (7) can be expressed as function of anchor $\mathbf{a}$ and hypothesized agent position $\tilde{\mathbf{p}}$. Furthermore, we employ (9) for the amplitude in (7) which enables to define the likelihood function parametrized solely on the hypothesized agent position $\tilde{\mathbf{p}}$, such that

$$L^{\mathrm{sa}}(\mathbf{r}_m; \tilde{\mathbf{p}}) \triangleq L^{\mathrm{sa}}(\mathbf{r}_m; \hat{\boldsymbol{\alpha}}_m^{\mathrm{sa}}, \boldsymbol{\tau}, \boldsymbol{\phi}). \quad (12)$$

It is an interesting finding that antenna m's beampattern affects the estimation of the amplitudes in (10) but its impact is canceled out once we plug the amplitude estimate in the likelihood function (12). Hence, the direction information provided by the beampatterns cannot be used when only a single-antenna measurement is considered.

2) Non-phase-coherent ML position estimate: We proposed to employ the ML criterion to estimate the agent position using the measured $\mathbf{r}_m$. Keeping in mind that at non-phase-coherent measurements the phase-offsets $e^{j\varphi_m}$ are inaccessible, the MPC amplitudes need to be estimated for each m independently. Therefore, we define the non-phase-coherent position estimate $\hat{\mathbf{p}}^{\mathrm{ncoh}}$ which maximizes the sum of the single-antenna log likelihood functions according to

$$\hat{\mathbf{p}}^{\mathrm{ncoh}} = \arg\max_{\tilde{\mathbf{p}}} \sum_{m=1}^{M} L^{\mathrm{sa}}(\mathbf{r}_m; \tilde{\mathbf{p}}). \quad (13)$$

Since the non-phase-coherent likelihood function has no access to angle information, the main information source are
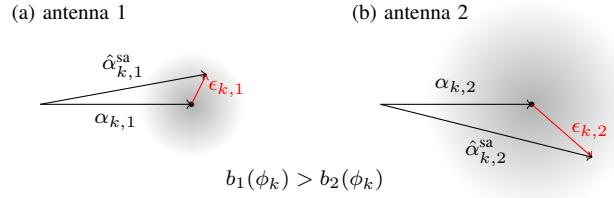
Fig. 2. Illustration of single-antenna amplitude estimate comparing antennas $m = 1$ (a) and $m = 2$ (b) where $b_1(\phi_k) > b_2(\phi_k)$. As shown in (11) the amplitude estimates can be decomposed into a true α_k plus an additive noise term $\epsilon_{k,m} = \frac{1}{b_m(\phi_k)} \mathbf{s}_{\tau_k}^H \mathbf{w}_m / \|\mathbf{s}_{\tau_k}\|^2$ which is zero-mean complex Gaussian distributed (indicated by the black circles). The increased amplitude gain by the beampattern of (a) compared to (b) is reflected in a more robust amplitude estimation.

the MPC delays which are used to find the agent position (see Figure 1). Maximization of $\sum_{m=1}^{M} L^{\mathrm{sa}}(\mathbf{r}_m; \tilde{\mathbf{p}})$ requires the evaluation of $\tilde{\mathbf{p}}$ at feasible positions (e.g. any point in the communication range to the anchor). Note that each $L^{\mathrm{sa}}(\mathbf{r}_m; \tilde{\mathbf{p}})$ employs a local amplitude estimate $\boldsymbol{\alpha}_m^{\mathrm{sa}}$ which limits the potential performance gain of (13). In the following we derive a position estimate seeking for a global $\boldsymbol{\alpha}$.

C. Phase-coherent ML estimate

1) Likelihood function for multiple antennas: Deriving a likelihood function for multiple antennas is straightforward. Each antenna measurement provides additional information of the MPC amplitudes. Hence, we can model the channel measurements as

$$\mathbf{r} = \boldsymbol{\Phi} \mathbf{X} \boldsymbol{\alpha} + \mathbf{w} \quad (14)$$

with

$$\mathbf{r} = \begin{bmatrix} \mathbf{r}_1 \\ \vdots \\ \mathbf{r}_M \end{bmatrix}, \boldsymbol{\Phi} = \begin{bmatrix} e^{j\varphi_1} \mathbf{I}_{N \times N} & & 0 \\ & \ddots & \\ 0 & & e^{j\varphi_M} \mathbf{I}_{N \times N} \end{bmatrix}$$

$$\mathbf{X} = \begin{bmatrix} \mathbf{X}_1 \\ \vdots \\ \mathbf{X}_M \end{bmatrix} = \begin{bmatrix} b_1(\phi_1)\mathbf{s}_{\tau_1} & \ldots & b_1(\phi_K)\mathbf{s}_{\tau_K} \\ \vdots & & \vdots \\ b_M(\phi_1)\mathbf{s}_{\tau_1} & \ldots & b_M(\phi_K)\mathbf{s}_{\tau_K} \end{bmatrix}, \mathbf{w} = \begin{bmatrix} \mathbf{w}_1 \\ \vdots \\ \mathbf{w}_M \end{bmatrix}$$

where $\boldsymbol{\Phi} \in \mathbb{C}^{MN \times MN}$ accounts for the phase-offsets. From (14) the values in $\mathbf{r}$ are distributed as complex Normal $\mathcal{N}(\boldsymbol{\Phi} \mathbf{X} \boldsymbol{\alpha}, \sigma^2 \mathbf{I}_{MN \times MN})$. The log likelihood function $L^{\mathrm{ma}}(\mathbf{r}; \tilde{\mathbf{p}})$ for multiple antennas is derived equivalent to the single-antenna ones according to

$$L^{\mathrm{ma}}(\mathbf{r}; \tilde{\mathbf{p}}) = -\frac{1}{\sigma^2}(\mathbf{r} - \boldsymbol{\Phi} \mathbf{X} \hat{\boldsymbol{\alpha}}^{\mathrm{ma}})^H (\mathbf{r} - \boldsymbol{\Phi} \mathbf{X} \hat{\boldsymbol{\alpha}}^{\mathrm{ma}}) \quad (15)$$

with amplitude estimate

$$\hat{\boldsymbol{\alpha}}^{\mathrm{ma}} = (\mathbf{X}^H \mathbf{X})^{-1} \mathbf{X}^H \boldsymbol{\Phi}^H \mathbf{r}. \quad (16)$$

In contrast to (12), the multiple antenna likelihood takes advantage of the beampattern (contained in $\mathbf{X}$) but requires a known phase-offset $\boldsymbol{\Phi}$.

To get more insight in the derived likelihood function, we assume non-overlapping MPCs which enables to rewrite (16) as

$$\hat{\alpha}_k = c \sum_{m=1}^{M} e^{-j\varphi_m} b_m^*(\phi_k) \mathbf{s}_{\tau_k}^H \mathbf{r}_m. \tag{17}$$

with normalization factor

$$c = \frac{1}{\displaystyle\sum_{m=1}^{M} |b_m(\phi_k)|^2 \|\mathbf{s}_{\tau_k}\|^2} \tag{18}$$

The sum on the right-hand-side of (17) can be interpreted as weighted average of the projection of the measured signal $\mathbf{r}_m$ onto the delayed, transmitted signal $\mathbf{s}_{\tau_k}$. The beampattern $b_m^*(\phi_k)$ accounts for the weighting and the phase-offset $e^{-j\varphi_m}$ is required for phase-coherent averaging.

To give an impression regarding the relation between single and multiple antenna amplitude estimates, we identify (10) in (17) yielding

$$\hat{\alpha}_k = c \sum_{m=1}^{M} e^{-j\varphi_m} \|\mathbf{s}_{\tau_k}\|^2 |b_m(\phi_k)|^2 \hat{\alpha}_{k,m}^{\mathrm{sa}}. \tag{19}$$

Hence, $\hat{\alpha}_k$ can be interpreted as weighted average of the single-antenna amplitudes $\hat{\alpha}_{k,m}^{\mathrm{sa}}$. The weighting by the beampattern counteracts the adverse effect of noise gain in (11).

2) Phase-coherent position estimate: Having phase-coherent measurements at hand, i.e. φ_m are known, we can obtain $L^{\mathrm{ma}}(\mathbf{r}; \tilde{\mathbf{p}})$, and the estimated agent position $\hat{\mathbf{p}}^{\mathrm{coh}}$ follows accordingly

$$\hat{\mathbf{p}}^{\mathrm{coh}} = \arg\max_{\tilde{\mathbf{p}}} L^{\mathrm{ma}}(\mathbf{r}; \tilde{\mathbf{p}}). \tag{20}$$

We can conclude that the amplitudes in $L^{\mathrm{ma}}(\mathbf{r}; \tilde{\mathbf{p}})$ are estimated in a phase-coherent fashion. Thus, the vital beampattern information became accessable but its deployment is limited to known phase-offsets.

III. BEAMPATTERN ASSISTED NON-PHASE-COHERENT POSITION ESTIMATE

In this work we make use of the antenna beampattern and simultaneously consider the phase-offset as nuisance. We propose to use (13) but exchange the amplitude estimation (9) by considering a weighted average of amplitudes, similar to (17). Rather than processing the complex-valued beampattern information, we propose to average only the absolute values and keep the noisy phase of the individual measurements [14].

We define an optimization problem, motivated by (13), according to

$$\hat{\mathbf{p}}^{\mathrm{pro}} = \arg\max_{\tilde{\mathbf{p}}} \sum_{m=1}^{M} \ell^{\mathrm{pro}}(\mathbf{r}_m; \tilde{\mathbf{p}}) \tag{21}$$

where ℓ^{pro} follows similar to (7) as

$$\ell^{\mathrm{pro}}(\mathbf{r}_m; \tilde{\mathbf{p}}) = -\frac{1}{\sigma^2}(\mathbf{r}_m - \mathbf{X}_m \boldsymbol{\alpha}_m^{\mathrm{avg}})^H (\mathbf{r}_m - \mathbf{X}_m \boldsymbol{\alpha}_m^{\mathrm{avg}}). \tag{22}$$

The required amplitudes $\boldsymbol{\alpha}_m^{\mathrm{avg}}$ are estimated as follows.

A. Estimation of amplitudes

We aim at calculating MPC amplitudes $\boldsymbol{\alpha}_m^{\mathrm{avg}}$ for each m which preserve the phase-offset of m while considering their beampattern. Let $\boldsymbol{\alpha}_m^{\mathrm{avg}} = [\alpha_{1,m}^{\mathrm{avg}}, \ldots, \alpha_{K,m}^{\mathrm{avg}}]^T$ then the amplitude of the kth MPC and mth antenna follows as

$$\alpha_{k,m}^{\mathrm{avg}} = |\alpha_k^{\mathrm{avg}}| e^{j\angle \alpha_{k,m}^{\mathrm{sa}}}. \tag{23}$$

We propose to estimate the amplitude's absolute value $|\alpha_k^{\mathrm{avg}}|$ and corresponding phase $e^{j\angle \alpha_{k,m}^{\mathrm{sa}}}$ independently[1]. Starting with $|\alpha_k^{\mathrm{avg}}|$ we seek for a weighted average using the provided beampattern information. Motivated by the phase-coherent amplitude estimate in (19) we exchange the complex-valued average by an absolute-valued average, by defining

$$|\alpha_k^{\mathrm{avg}}| \triangleq c \sum_{m=1}^{M} \left| e^{-j\varphi_m} \|\mathbf{s}_{\tau_k}\|^2 |b_m(\phi_k)|^2 \hat{\alpha}_{k,m}^{\mathrm{sa}} \right|$$

$$= c \sum_{m=1}^{M} \|\mathbf{s}_{\tau_k}\|^2 |b_m(\phi_k)|^2 |\hat{\alpha}_{k,m}^{\mathrm{sa}}|. \tag{24}$$

Having a weighted average of amplitudes, the corresponding phase $e^{j\angle \alpha_{k,m}^{\mathrm{sa}}}$ follows from the single-antenna estimates (9).

B. Insights

We are interested in the behavior of the amplitude approximation (23). Plugging (10) and (24) in (23) results in

$$\alpha_{k,m}^{\mathrm{avg}} = c e^{j\angle b_m^*(\phi_k) \mathbf{s}_{\tau_k}^H \mathbf{r}_m} \sum_{m'=1}^{M} |b_{m'}^*(\phi_k) \mathbf{s}_{\tau_k}^H \mathbf{r}_{m'}| \tag{25}$$

and plugging (4) in (25) yields

$$\alpha_{k,m}^{\mathrm{avg}} = \alpha_k e^{j\varphi_m} \chi_{k,m} \tag{26}$$

where the multiplicative term $\chi_{k,m}$ accounts for the induced error due to the approximation in (23). In case of non-overlapping MPCs, $\chi_{k,m}$ can be formulated as

$$\chi_{k,m} = \frac{\displaystyle\sum_{m'=1}^{M} |b_{m'}(\phi_k)|^2 \|\mathbf{s}_{\tau_k}\|^2 |1 + \xi_{k,m'}^{-1}|}{\displaystyle\sum_{m'=1}^{M} |b_{m'}(\phi_k)|^2 \|\mathbf{s}_{\tau_k}\|} e^{j\angle(1 + \xi_{k,m}^{-1})} \tag{27}$$

where $\xi_{k,m}$ can be interpreted similar to a signal to noise ratio as

$$\xi_{k,m} = \frac{e^{j\varphi_m} b_m(\phi_k) \alpha_k \|\mathbf{s}_{\tau_k}\|^2}{\mathbf{s}_{\tau_k}^H \mathbf{w}}. \tag{28}$$

It can be shown that for increasing $\xi_{k,m}$ the error term $\chi_{k,m}$ attains a value of one showing that $\alpha_{k,m}^{\mathrm{avg}}$ asymptotically attains the true $e^{j\varphi_m} \alpha_k$

$$\alpha_{k,m}^{\mathrm{avg}} \xrightarrow{\xi_{k,m} \to \infty} e^{j\varphi_m} \alpha_k \tag{29}$$

In case of overlapping MPCs $\xi_{k,m}$ contains additional cross terms stemming from $\mathbf{s}_{\tau_k}^H \mathbf{X}_m$ in (25). These cross terms can be interpreted as additional bias in $\xi_{k,m}$ which hinders to attain to the true amplitudes.

---

[1] An iterative optimization scheme would be necessary to estimate a single φ_m per antenna and use (16) to estimate the complex amplitudes. Thus we opted for the simple closed-form expression presented above.

phase-coherent $L^{\mathrm{ma}}(\mathbf{r}; \tilde{\mathbf{p}})$ non-phase-coherent $\sum_m L^{\mathrm{sa}}(\mathbf{r}_m; \tilde{\mathbf{p}})$ proposed $\sum_m \ell^{\mathrm{pro}}(\mathbf{r}_m; \tilde{\mathbf{p}})$
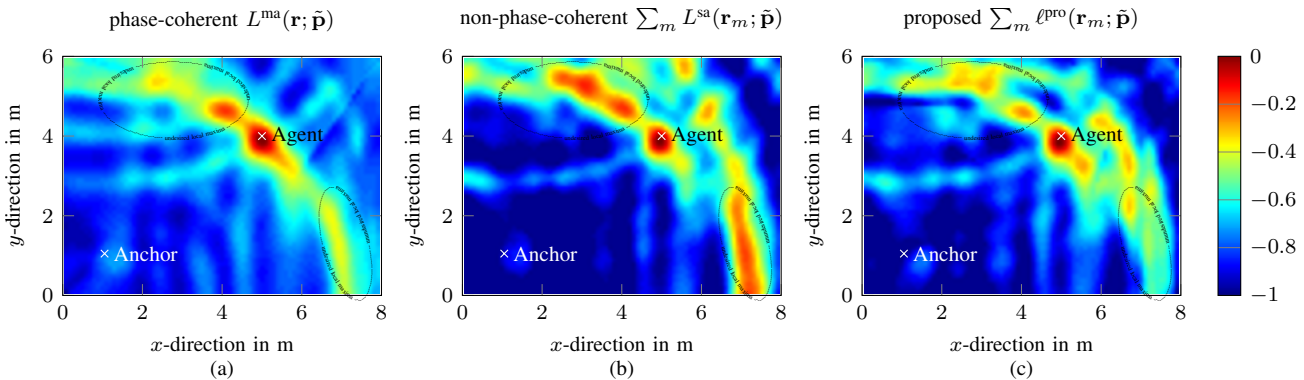
Fig. 3. Evaluated log likelihood function $L^{\mathrm{ma}}(\mathbf{r}; \tilde{\mathbf{p}})$, shown in (a), $\sum_m L^{\mathrm{sa}}(\mathbf{r}_m; \tilde{\mathbf{p}})$ (b) and $\sum_m \ell^{\mathrm{pro}}(\mathbf{r}_m; \tilde{\mathbf{p}})$ (c) for various positions $\tilde{\mathbf{p}}$. The coherent amplitude estimate in (16) (a) utilizes the antennas beampattern which results in a strong global maximum at the true agent position while suppressing neighboring local maxima. The independent estimation of the MPC amplitudes, shown in (b), ignores the vital information provided by the beampattern, resulting in several strong local maxima in the likelihood function. Averaging of absolute MPC amplitudes using (24) (c) reveals a performance gain compared to independent estimation (Fig. 3b). Local maxima are strongly reduced and the global maximum is clearly located at the agent's true location.

C. Implementation

The amplitudes used in (22) are calculated using (23) where the elements $\hat{\alpha}_{k,m}^{\mathrm{sa}}$ in (23) and (24) are taken from the single-antenna measurements using (9). Note, overlapping multipath is reflected in non-orthogonal columns in $\mathbf{X}_m$ troubling the matrix inversion in (9). Therefore, in case of path overlap we exchange (9) and estimate the amplitudes iteratively as explained in the following: Starting with the first MPC $k = 1$ we estimate only one amplitude $\hat{\alpha}_{1,m}$ using (10). We continue by subtracting the estimated MPC $\hat{\alpha}_{1,m}\mathbf{s}_{\tau_1}$ from the measurement $\mathbf{r}_m$. Then, the second MPC's amplitude $\hat{\alpha}_{2,m}$ is estimated from $\mathbf{r}_m$ (where the first MPC is already subtracted). This procedure (estimation and subtraction) is continued until K is reached. In this way we can circumvent the issue of overlapping paths. We use the iterative amplitude estimation if there is at least one pair of MPC delays $\tau_k, \tau_{k'}$ with (heuristically chosen) distance below $|\tau_k - \tau_{k'}| < \frac{1}{4}T_{\mathrm{p}}$ with pulse duration T_{p}.

A comparison in terms of computational costs reveals similar complexity of the proposed method and the non-phase-coherent method. Additional costs are justified by the MK multiplications in (23) and K times $M - 1$ multiply and add operations in (24).

IV. EVALUATION

Our evaluation is twofold. First, we provide a qualitative comparison of the derived likelihood functions and proceed with a quantitative evaluation of the achieved position accuracy. For the evaluation of the likelihood functions we generated an indoor scenario with an anchor located at $\mathbf{a} = [1,1]^T$ m and an agent at $\mathbf{p} = [5,4]^T$ m, both placed inside a rectangular room with dimensions 8×6 m. To ensure a realistic scenario we employ the directive antenna from [7] with known complex-valued beampattern $b_m(\phi)$ scaled to $\max_\phi |b_m(\phi)| = 1$. The antenna's half-power beamwidth is roughly $90°$ along the azimuth angle. We use $M = 4$ antennas, circularly assembled in $360°/M = 90°$ steps. The multipath parameters are obtained as follows: the MPC delay and angle are calculated using the geometry model in [13]. The MPC amplitude is attenuated by -3 dB at each reflection point.

The path loss is considered using Friis' equation which scales the amplitude with the inverse of the path length. We model single reflections resulting in a line-of-sight (LOS) plus four reflections. As transmitted pulse we employ a raised cosine signal with $T_{\mathrm{p}} = 2.4$ ns and roll-off factor $R = 0.9$, sampled at $T_s = 1.0016$ ns. Note, in [15] those parameters were identified to describe IEEE 802.15.4 (2011) Channel 2 of the DecaWave DW1000 UWB radio. The variance $\sigma^2 = N_0/T_s$ of the Gaussian noise $w_m[n]$ was set to a signal-to-noise-ratio $\frac{|\alpha|^2 \|\mathbf{s}_\tau\|^2}{N_0}$ equal to 30 dB for a path distance of 1 m.

The derived position estimates $\hat{\mathbf{p}}^{\mathrm{coh}}$, $\hat{\mathbf{p}}^{\mathrm{ncoh}}$ and $\hat{\mathbf{p}}^{\mathrm{pro}}$ are based on the likelihoods in (15), (12) and (22), respectively, which justifies the importance of well-conditioned likelihood functions, i.e. single unique maxima while suppressing neighboring local maxima. In this qualitative comparison we illustrate the likelihood functions for the phase-coherent in (15) (Figure 3a) and non-phase-coherent case $\sum_m L^{\mathrm{sa}}(\mathbf{r}_m; \tilde{\mathbf{p}})$ (Figure 3b) in comparison with the proposed method $\sum_m \ell^{\mathrm{pro}}(\mathbf{r}_m; \tilde{\mathbf{p}})$ (Figure 3c).

The comparison between the phase-coherent and non-phase-coherent likelihood functions (Figures 3a and 3b) reveals the importance of the beampattern, used in $L^{\mathrm{ma}}(\mathbf{r}; \tilde{\mathbf{p}})$. Its outcome is characterized by a strong global maxima at the true agent position. Local maxima in the vicinity of the true agent position are strongly suppressed. This enables a reliable position estimate using the ML scheme (15) applied to $L^{\mathrm{ma}}(\mathbf{r}; \tilde{\mathbf{p}})$. In contrast, the likelihood $\sum_m L^{\mathrm{sa}}(\mathbf{r}_m; \tilde{\mathbf{p}})$ for non-phase-coherent suffers due to the inaccessible beampattern information resulting in several local maxima in $\sum_m L^{\mathrm{sa}}(\mathbf{r}_m; \tilde{\mathbf{p}})$. These local maxima deteriorate the position accuracy especially at low SNRs.

The proposed method $\sum_m \ell^{\mathrm{pro}}(\mathbf{r}_m; \tilde{\mathbf{p}})$ employs the approximation in (23) to make use of the beampattern while preserving non-phase-coherent processing. The fair comparison between both non-phase-coherent methods in Figures 3b and 3c shows the potential performance gain. The global maximum is clearly visible at the true agent position and neighboring local maxima are suppressed. The remarkable likelihood outcome attains a similar performance as $L^{\mathrm{ma}}(\mathbf{r}; \tilde{\mathbf{p}})$

(Fig. 3) without the need of phase-coherent processing.

We proceed with a quantitative evaluation of the proposed algorithm in comparison with phase-coherent position estimates. We randomly place the agent position $\mathbf{p}$ inside the rectangular room from the previous evaluation and keep the anchor node fixed at $\mathbf{a} = [1, 1]^T$ m. We repeat the experiment 1000 times and calculate the ML solutions $\hat{\mathbf{p}}^{\mathrm{coh}}$, $\hat{\mathbf{p}}^{\mathrm{ncoh}}$ and $\hat{\mathbf{p}}^{\mathrm{pro}}$. Furthermore, we compute a lower bound on the root mean square position error based on the Cramér-Rao inequality at each of the evaluated positions. We evaluated the functions for points $\tilde{\mathbf{p}}$ on a grid with 25×25 cm spacing, resulting in 9 sampling points/m^2. Figure 4 exemplifies the cumulative distribution function (CDF) of the position error. The phase-coherent position estimate $\hat{\mathbf{p}}^{\mathrm{coh}}$ (dashed, black) achieves the smallest position errors due to its access to known phase-offsets. Both $\hat{\mathbf{p}}^{\mathrm{ncoh}}$ (dash-dotted, green) and $\hat{\mathbf{p}}^{\mathrm{pro}}$ (solid, blue) are based on non-coherent processing. This information loss leads to a performance degradation especially for $\hat{\mathbf{p}}^{\mathrm{ncoh}}$. In contrast, the results of the proposed method outperform the competitive method $\hat{\mathbf{p}}^{\mathrm{ncoh}}$, and is able to diminish the gap towards the results of $\hat{\mathbf{p}}^{\mathrm{coh}}$ without the requirement of known phase-offsets.

Finally, we employ the algorithms on real measured data, taken from [7]. The measurements were performed in a laboratory room with dimensions of 6×8 m, as illustrated in [7, Figure 1]. For a fair comparison we choose same signal parameters $T_\mathrm{p} = 2.4$ ns, $R = 0.9$ and carrier frequency $f_c = 5.4$ GHz as in [7]. The CDF of the position error is shown in Fig. 5. The proposed method (solid, blue) outperforms the non-phase-coherent position estimate (dash-dotted, green). Although no access to phase-offsets is provided, the proposed method is able to approach the phase-coherent position estimate (dotted, black) with only a minor performance loss. We can observe that 90 % of the errors are below 40 cm.

From our results based on real and computer generated data we can conclude that the additional costs for phase-coherent measurements need to be carefully reconsidered when facing the outperforming results of the proposed method.

V. CONCLUSION

In this work we have developed an algorithm capable of high-accuracy indoor positioning, demanding a single-anchor setup only. We elaborate the impact of phase-coherent measurements for joint MPC amplitude estimates. Our analysis unveiled the possibility to circumvent the necessity of phase-coherent measurements while minimizing the penalty on the position performance.

Fig. 4. CDF of phase-coherent $\hat{\mathbf{p}}^{\mathrm{coh}}$, non-phase-coherent $\hat{\mathbf{p}}^{\mathrm{ncoh}}$ and of the proposed position estimate $\hat{\mathbf{p}}^{\mathrm{pro}}$ using computer generated data.
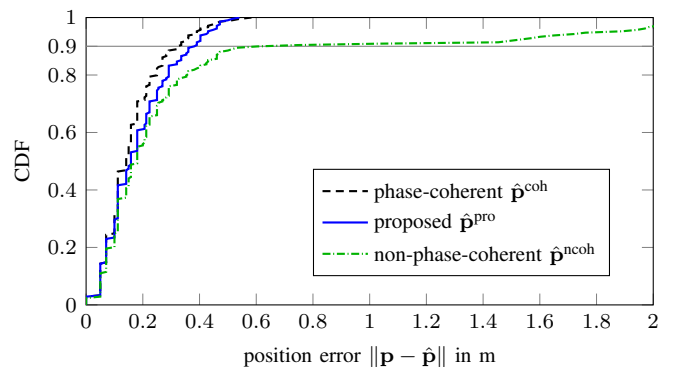
Fig. 5. CDF of phase-coherent $\hat{\mathbf{p}}^{\mathrm{coh}}$, non-phase-coherent $\hat{\mathbf{p}}^{\mathrm{ncoh}}$ and of the proposed position estimate $\hat{\mathbf{p}}^{\mathrm{pro}}$ using measured data from [7].

REFERENCES

[1] Y. Shen and M. Z. Win, "Fundamental limits of wideband localization-part I: A general framework," vol. 56, no. 10, pp. 4956–4980, Oct. 2010.

[2] E. Leitinger, P. Meissner, C. Rudisser, G. Dumphart, and K. Witrisal, "Evaluation of position-related information in multipath components for indoor positioning," *IEEE JSAC*, vol. 33, no. 11, pp. 2313–2328, Nov. 2015.

[3] P. Meissner, D. Arnitz, T. Gigl, and K. Witrisal, "Analysis of an indoor UWB channel for multipath-aided localization," in *IEEE Intern. Conf. on Ultra-Wideband, ICUWB*, Bologna, Italy, Sep. 2011.

[4] Y. Han, Y. Shen, X. P. Zhang, M. Z. Win, and H. Meng, "Performance limits and geometric properties of array localization," vol. 62, no. 2, pp. 1054–1075, Feb. 2016.

[5] G. Giorgetti, A. Cidronali, S. K. S. Gupta, and G. Manes, "Single-anchor indoor localization using a switched-beam antenna," *IEEE Communications Letters*, vol. 13, no. 1, pp. 58–60, January 2009.

[6] H. Zhang, X. Cui, B. An, and T. A. Gulliver, "A distance and angle estimated method based on single UWB station," in *2013 IEEE International Conference on Signal Processing, Communication and Computing (ICSPCC 2013)*, Aug 2013, pp. 1–6.

[7] M. Rath, J. Kulmer, M. S. Bakr, B. Großwindhager, and K. Witrisal, "Multipath-assisted indoor positioning enabled by directional UWB sector antennas," in *18th IEEE International Workshop on Signal Processing Advances in Wireless Communications, SPAWC*, 2017.

[8] BeSpoon, *UM100 Evaluation Kit Quick Start Guide*, BeSpoon, 2015.

[9] DecaWave, *DW1000 User Manual, Version 2.05*, DecaWave, 2015.

[10] K. Witrisal *et al.*, "High-accuracy localization for assisted living: 5g systems will turn multipath channels from foe to friend," *IEEE MSP*, vol. 33, no. 2, pp. 59–70, March 2016.

[11] J. B. Allen and D. A. Berkley, "Image method for efficiently simulating small-room acoustics," *The Journal of the Acoustical Society of America*, vol. 65, no. 4, pp. 943–950, 1979.

[12] J. Borish, "Extension of the image model to arbitrary polyhedra," *The Journal of the Acoustical Society of America*, vol. 75, no. 6, 1984.

[13] J. Kulmer, E. Leitinger, S. Grebien, and K. Witrisal, "Anchorless cooperative tracking using multipath channel information," *IEEE Transactions on Wireless Communications, in press*, 2018.

[14] P. Mowlaee, J. Kulmer, J. Stahl, and F. Mayer, *Single Channel Phase-Aware Signal Processing in Speech Communication: Theory and Practice*. Wiley, 2016.

[15] J. Kulmer, S. Hinteregger, B. Grosswindhager, M. Rath, M. Bakr, E. Leitinger, and K. Witrisal, "Using DecaWave UWB transceivers for high-accuracy multipath-assisted indoor positioning," in *IEEE ICC Workshop on Advances in Network Localization and Navigation (ANLN)*, pp. 219–225, France, May 2017.